Fish Method based on-line optimal control for PWM Rectifiers

André Veltman[1]
Univ. of Wisconsin, Madison, Dept. of Mech. Eng.
1513 University Avenue
Madison, WI 53706, USA
e-mail: a.veltman@ele.tue.nl

Jorge L. Duarte[1]
[1]Eindhoven University of Technology
Electromechanics and Power Electronics Group
P.O. Box 513
5600 MB Eindhoven, The Netherlands

***Abstract*— A control strategy for hard switching high power PWM rectifiers, based on carrier-less Volt-second (flux) control is presented. Insights from the Fish Method yield switching rules in the synchronous frame such that, even during major setpoint changes, none of the switches ever violates a pre-determined minimum pulse width. The control method realizes outstanding transient behaviour at low switching frequencies and allows a small DC-link capacitance, low inductance loads as well as non-equal dwell-times. Experimental data of a small DSP-controlled 1 [kW] IGBT PWM rectifier is presented.**

I. Introduction

The control of an inverter as a motor drive or as a Pulse Width Modulated (PWM) rectifier is basically the same. A running machine can be considered as a per phase voltage source (the back-EMF), a leakage inductance and some stator resistance. In a similar way, the utility grid can be considered as a per phase stiff voltage source. If we connect series inductors L between the grid and *Inverter 1* in fig.1a, it appears as if the inverter drives an infinitely large machine (constant speed) with a known leakage inductance L and some resistance R.

Instead of the usual voltage based control, in this paper the inverters as shown in fig.1a are flux controlled. Both inverters are identical two-level inverters and consist of 3 inverter legs that can be switched independently to either the + terminal of the DC link ('1') or to the − terminal ('0'). While controlling the inverter, only $2^3 = 8$ different switching states can be used, yielding 6 separate active vectors and two zero vectors (000 and 111) as shown in fig.1c.

The linked inverter flux $\vec{\Psi}^s_{inv}$ in the stationary frame (which is indicated by $(..)^s$, using α, β coordinates) equals the time integral of the inverter voltage vector $\vec{u}^s_{inv}$. Flux

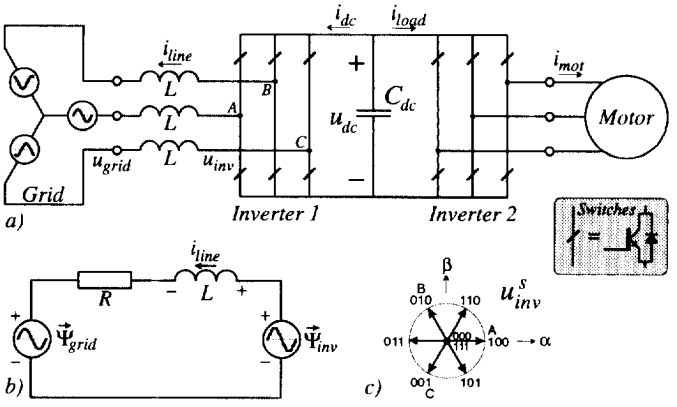

Fig. 1. a) Lay-out of AC-DC-AC configuration. b) Flux model in stationary frame. c) Inverter voltage vectors for all $2^3 = 8$ combinations.

$\vec{\Psi}^s_{inv}$ is a continuous variable and therefore well suited to use as a feed-back signal.

$$\vec{\Psi}^s_{inv} = \vec{\Psi}^s_{inv}(0) + \int_0^t \vec{u}^s_{inv}(\tau)d\tau \tag{1}$$

From a current point of view it is now very easy to show how the current $\vec{i}^s_{line}$ is generated as a function of the two voltages on either end of inductor L. When we neglect the resistance R, the current equation becomes an analytic expression in terms of inverter flux and grid flux $\vec{\Psi}^s_{grid}$:

$$\vec{i}^s_{line} = \frac{\vec{\Psi}^s_{inv} - \vec{\Psi}^s_{grid}}{L} \tag{2}$$

The grid flux $\vec{\Psi}^s_{grid}$ cannot be estimated by means of open-loop integration of $\vec{u}^s_{grid}$ in practise. Instead a special integrator structure with transfer function $H(s)$ is used in (3). The transfer function expressed in the Laplace operator s has a large gain around 1 [Hz], but zero gain

0-7803-2730-6/95 $4.00 © 1995 IEEE

at DC, and mimics a 'pure integrator' adequately for all frequencies above 5 [Hz], including the grid frequency.

$$\vec{\Psi}^s_{grid}(s) = \frac{s\tau_a}{(s\tau_b+1)(s\tau_c+1)} \cdot \vec{u}^s_{grid}(s) \qquad (3)$$

The system in fig.1 can be robustly controlled when the power flow into the link capacitor C_{dc} can be kept at a zero average, regardless all allowable excursions of i_{load}. The zero average should be maintained on a timescale larger than that of the switching ripple. In practise the capacitor C_{dc} will allow power unbalance for at least a few milli-seconds before the voltage u_{dc} goes out of bounds. Power flow P_{grid} from *Inverter 1* towards the grid equals the scalar product of line current vector and line voltage vector, or when expressed in terms of flux, as the vector product between $\vec{i}^s_{line}$ and grid flux $\vec{\Psi}^s_{grid}$:

$$P_{grid} = \vec{i}^s_{line} \cdot \vec{u}^s_{grid} = (-\vec{i}^s_{line} \times \vec{\Psi}^s_{grid})\omega_{grid} \qquad (4)$$

The term between brackets in (4) equals the additional torque on the generator that feeds the grid. When losses in *Inverter 1* are neglected we can also define the power P_{dc} from the link to the grid:

$$P_{dc} = i_{dc} \cdot u_{dc} = P_{grid} \qquad (5)$$

$$P_{load} = i_{load} \cdot u_{dc} \qquad (6)$$

The control objective for *Inverter 1* is to keep u_{dc} constant at a predefined value and to adjust P_{grid} in the best possible way to match $-P_{load}$ and the losses.

II. The Fish Method

The name *Fish Method* [5] originates from the fact that flux vectors and current vectors of certain switching patterns of Inverters create graphs that resemble the shape of a fish. This section shows a measured data set of an inverter driving a 45 [kW] induction motor, presented in both the stationary and synchronous frames. The main advantage of using flux vectors instead of voltage vectors, is that flux magnitude is independent of the coordinate system it is represented in. Because linked flux and current depend linearly (2), all equations involving just current and flux can be written in any reference frame without causing cross coupling products.

The *fish method* incorporates a coordinate transformation of $\vec{\Psi}^s_{inv}$ and $\vec{i}^s_{mot}$ onto a revolving coordinate system which is attached to the fundamental frequency component of $\vec{\Psi}^s_{inv}$. The *fish* transformation is defined as the complex transformation $e^{-j\varphi}$, which performs a rotation over angle $-\varphi$. In steady-state $\varphi = \omega_{inv}t$, $(..)^f$ in a,b coordinates, indicates *fish* related reference in the synchronous frame.

$$\begin{pmatrix} \Psi^f_{inv\,a} \\ \Psi^f_{inv\,b} \end{pmatrix} = \begin{bmatrix} \cos(-\varphi) & -\sin(-\varphi) \\ \sin(-\varphi) & \cos(-\varphi) \end{bmatrix} \cdot \begin{pmatrix} \Psi^s_{inv\,\alpha} \\ \Psi^s_{inv\,\beta} \end{pmatrix} \qquad (7)$$

Or in complex notation for both flux and current:

$$\vec{\Psi}^f_{inv} = e^{-j\varphi} \cdot \vec{\Psi}^s_{inv} \qquad \vec{i}^f_{mot} = e^{-j\varphi} \cdot \vec{i}^s_{mot} \qquad (8)$$

The shape of $\vec{\Psi}^f_{inv}$ is fully determined by the applied switching pattern and represents the overall effect of all higher (flux) harmonics combined. The average value of $\vec{\Psi}^f_{inv}$ represents the fundamental component of $\vec{\Psi}^s_{inv}$.

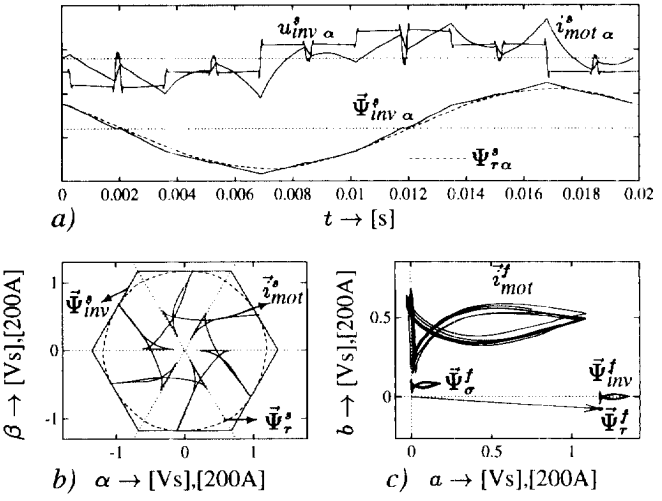

Fig. 2. Measured data: $\vec{i}^s_{mot}$ and $\vec{u}^s_{inv}$ of a 80 [kVA] forced commutated voltage source thyristor converter driving a 45 [kW] induction motor. Stator frequency: 50.56 [Hz] loaded by DC-generator, Estimated: $L = 0.88$ [mH], $\vartheta = 3.65°$.

In steady-state, the rotor flux vector $\vec{\Psi}^s_r$, an approximately uniformly revolving vector in stationary frame, becomes a virtually stationary vector in fish coordinates with magnitude Ψ_r and loading angle ϑ, relative to the a axis (fig.2c). In general the load angle $\vartheta > 0$ for driving mode. In generator mode $\vartheta < 0$. The no-load condition corresponds to $\vartheta \approx 0$.

$$\begin{pmatrix} \Psi^f_{r\alpha} \\ \Psi^f_{rb} \end{pmatrix} = \Psi_r \cdot \begin{pmatrix} \cos\vartheta \\ -\sin\vartheta \end{pmatrix} \qquad (9)$$

In the idealized case of zero stator resistance: $R_S = R = 0$, the simplified machine model in fig.1b, replacing

$\vec{\Psi}^s_{grid}$ by $\vec{\Psi}^s_r$, gives an analytical expression for the stator current vector $\vec{i}^s_{mot}$, similar to (2). In this case inductance L represents the total leakage inductance of the induction motor.

$$\vec{i}^s_{mot}\Big|_{R=0} = \frac{\vec{\Psi}^s_\sigma}{L} = \frac{\vec{\Psi}^s_{inv} - \vec{\Psi}^s_r}{L} \tag{10}$$

Magnitudes of and relative angles between flux vectors are conserved in fish coordinates, thus (10) can be transformed into:

$$\vec{i}^f_{mot}\Big|_{R=0} = \frac{\vec{\Psi}^f_\sigma}{L} = \frac{\vec{\Psi}^f_{inv} - \vec{\Psi}^f_r}{L} \tag{11}$$

An illustration of the above steps on measured data is given in fig.2a. The fact that the machine current vector is directly related to the integrated stator voltage vector is not so obvious in fig.2b; The hexagon $\vec{\Psi}^s_{inv}$ and the 'star' $\vec{i}^s_{mot}$ do not look alike. However, when these related quantities are represented in the synchronous frame, their similar 'fish-like' shape in fig.2c is evident. The ratio between the sizes of $\vec{\Psi}^f_s$ and $\vec{i}^f_{mot}$ reveals the effective leakage inductance L because $\vec{\Psi}^f_r$ is indeed almost a constant vector and hardly affects the fish shape of $\vec{\Psi}^f_\sigma$ (fig.2c).

A very important finding from the above analysis is that the inverter's switching pattern alone causes all current harmonics in the machine- or in the line-currents. To reduce harmonic currents, our goal should be to reduce the size of the flux fish $\vec{\Psi}^f_{inv}$ as much as possible.

III. Flux-control strategy

Still neglecting R, the line current in fig.1a,b is fully determined by fluxes (see (2) and (10)). The fluxes $\vec{\Psi}^s_{grid}$ and $\vec{\Psi}^s_{inv}$ are calculated by (3) and (1).

When power P_{load} is drawn by the load –whether by *Inverter 2* or any other load on the dc-link– the rectifier (*Inverter 1*) should provide compensating power to C_{dc} as soon as possible. The link voltage u_{dc} is controlled to have a constant average by means of a simple PI controller that asks additional power: $P_{control}$. The total power needed from the grid, P^*_{grid} also contains the estimated load power (6), the I^2R losses and the converter's switching losses (neglected in the next analysis).

$$P^*_{grid} = P_{load} + P_{control} + (I^2_{active} + I^2_{react}) \cdot R \tag{12}$$

$$I^* = \frac{P^*_{grid}}{U_{grid}} \tag{13}$$

When controlled, $I_{active} = I^*$, and $I_{react} = I^*_{react}$ hence (12) and (13) yield:

$$I^* = \frac{U_{grid} - \sqrt{U^2_{grid} - 4R \cdot P^*_{grid}}}{2R} \tag{14}$$

The active reference current I^* in (14) feeds forward the losses in R, leaving a smaller error for the u_{dc} controller to feed back. If the link capacitor is sufficiently large, the PI controller will eventually exactly compensate all load power and losses, even without the feed forward.

A. Steady state and dynamic control

In most cases unity powerfactor on the line-side of the rectifier is optimal. Unity powerfactor and (4) implies that $\vec{i}_{line}$ is perpendicular to the grid flux $\vec{\Psi}^s_{grid}$ and $I^*_{react} = 0$. The way the inverter flux Ψ^*_{inv} should be controlled relative to $\vec{\Psi}_{grid}$ is given in fig.3.

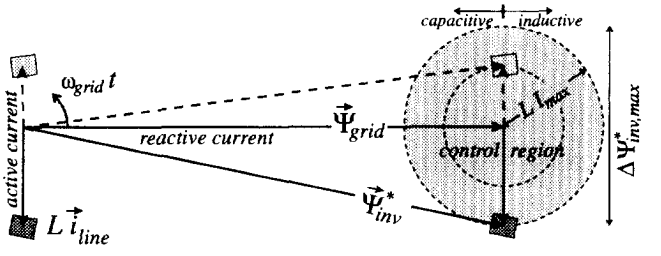

Fig. 3. Flux based control vector diagram in synchronous frame.

In case a non-unity powerfactor is required, line current $\vec{i}^s_{line}$ can be controlled leading (capacitive) or lagging (inductive) by means of either reducing or enlarging the reactive component of $\vec{\Psi}^*_{inv}$ respectively. The choice of the inductor value L is critical. First of all, a larger L will increase the flux difference needed to generate I_{max}: the control region increases proportional to L. An advantage is that the ripple current decreases with L. The gray box around the tip of Ψ^*_{inv} bounds the area to which $\vec{\Psi}_{inv}$ is constrained by the switching rules. All switches, whether GTO's or IGBT's, have a minimum pulse width T_{sw} to regard. The way the box's minimal dimensions depend on T_{sw}, u_{dc} and ω_{grid} is explained in later sections. It should be clear that the switch and snubber characteristics will allow a certain minimum size of the flux fish, regardless the size of L. The *rms* value of the flux deviations $\Delta\vec{\Psi}^f = \vec{\Psi}^f_{inv} - \vec{\Psi}^{f*}_{inv}$ will be more or less constant, hence the total harmonic distortion of the current at a given amplitude is inversely proportional to L.

However, when a relatively large L is used, the highest worst case transition of $\Delta\Psi^*_{inv}$ is also large. The worst case to think of, is when the load current i_{load} goes from positive maximal to negative maximal. In fig.3 can be seen that Ψ^*_{inv} has to pass $\vec{\Psi}_{grid}$ 'against the wind of the back-EMF' in order to change the sign of I_{line}. The amount of voltage available to move $\Psi^f_{inv\,b}$ equals $\sqrt{\frac{2}{3}}u_{dc} - U_{grid}$, thus the time to cross the control region in fig.3 from the bottom to the top will increase proportional with L. Supposing a stepwise change in i_{load}, the amount of electric charge Q to be supplied by the capacitor C_{dc} during this transition will also be approximately proportional to L. Hence, when a certain voltage droop or surge of Δu_{dc} on the steady state U_{dc} is allowed, the required capacitance C_{dc} roughly comes to:

$$C_{dc} \approx \frac{LI^2_{max}}{\Delta u_{dc}\left(\sqrt{\frac{2}{3}}U_{dc} - U_{grid}\right)} \tag{15}$$

The reference current vector in the stationary frame $\vec{i}^{s*}_{line}$ can be constructed when the angle ξ of $\vec{\Psi}^s_{grid}$ is known. The grid flux from (4) is sampled and translated to amplitude and angle with a digital *cartesian→polar* transformation.

$$\xi = \text{angle}(\vec{\Psi}^s_{grid}) \tag{16a}$$

$$\vec{i}^{s*}_{line} = I^* \cdot e^{\jmath(\xi - \frac{\pi}{2})} + I^*_{react} \cdot e^{\jmath\xi} \tag{16b}$$

The rectifier flux $\vec{\Psi}^{s*}_{inv}$ required to produce the reference current $\vec{i}^{s*}_{line}$ in (16b) is, including the flux across R:

$$\vec{\Psi}^{s*}_{inv} = L \cdot \vec{i}^{s*}_{line} + \int R \cdot \vec{i}^{s*}_{line}\, dt + \vec{\Psi}^s_{grid} \tag{17}$$

$$\Psi^*_{inv} = \|\vec{\Psi}^{s*}_{inv}\| \tag{18}$$

$$\cos\varphi = \frac{\Psi^{s*}_{inv\,\alpha}}{\Psi^*_{inv}} \qquad \sin\varphi = \frac{\Psi^{s*}_{inv\,\beta}}{\Psi^*_{inv}} \tag{19}$$

Once the required flux $\vec{\Psi}^{s*}_{inv}$ is known, the Fish Method comes into play. The measured voltages on the rectifier side of the L are integrated according to (1). This measured flux is projected onto the reference flux by means of a coordinate transformation using (19).

$$\vec{\Psi}^f_{inv} = \vec{\Psi}^s_{inv} \cdot e^{-\jmath\varphi} \tag{20}$$

The flux $\vec{\Psi}^f_{inv}$ is now controlled such that it never leaves a rectangular box [3] around Ψ^*_{inv} as depicted in fig.3 and fig.5.

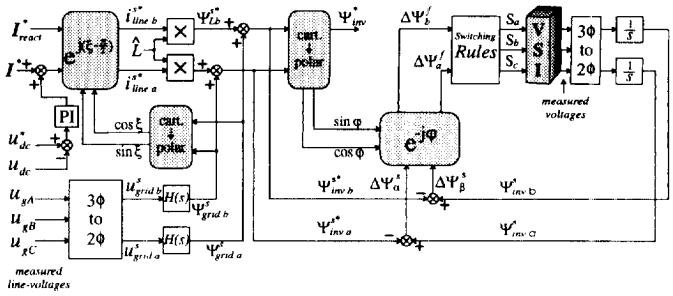

Fig. 4. Block diagram of DSP fish method PWM rectifier controller.

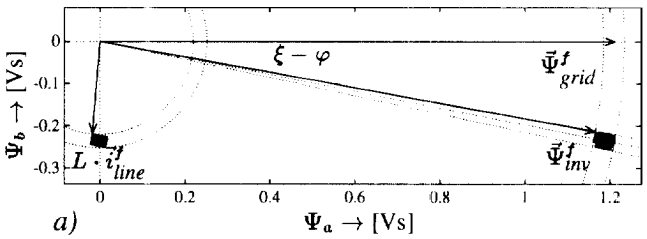

Fig. 5. Simulation: Vector diagram with Ψ^f_{grid}, flux-fish Ψ^f_{inv} and inductor flux-fish $L_{grid} \cdot I^f_{line}$, aligned to the grid flux. When $I^*_{react} = 0$ the current fish is on the $\alpha = 0$ axis.

IV. On line optimal switching strategy

From the theory about synchronous optimal switching patterns [4] was found that rectangular shaped flux fishes ($\vec{\Psi}^f_{inv}$) produce the smallest peak to peak current- and torque-ripple. When constraining the flux $\vec{\Psi}^f_{inv}$ in the synchronous frame, relative to the vector Ψ^*_{inv}, two bounded error-bands ε_r and ε_t apply. Therefore the flux fish $\vec{\Psi}^f_{inv}$ is confined to the area:

$$\vec{\Psi}^f_{inv} \in \Psi^*_{inv} \begin{pmatrix} 1 \pm \varepsilon_r \\ \pm\varepsilon_t \end{pmatrix} \tag{21}$$

The orbit shape of $\vec{\Psi}^s_{inv}$ at a switching pattern with constant reference flux amplitude Ψ^*_{inv} is either a hexagon or a polygon with $6+12N_T$ sides, where N_T equals the number of phase transitions per section of 30°, as shown in fig.6.

For each N_T, a global minimum for the radial error ε_r exists and is found analytically [5]. Only certain values of ε_r are optimal, given in table 1.

Fig.6 shows the optimized orbits, squeezed between the circles $\Psi^*_{inv} \cdot (1 - \varepsilon_r)$ and $\Psi^*_{inv} \cdot (1 + \varepsilon_r)$. The first simple switching rule can easily be formulated from the orbits in fig.6: When the orbit hits the outer circle, the next adjacent active vector is executed (+60°) and when the inner orbit is hit, the previous adjacent active vector is

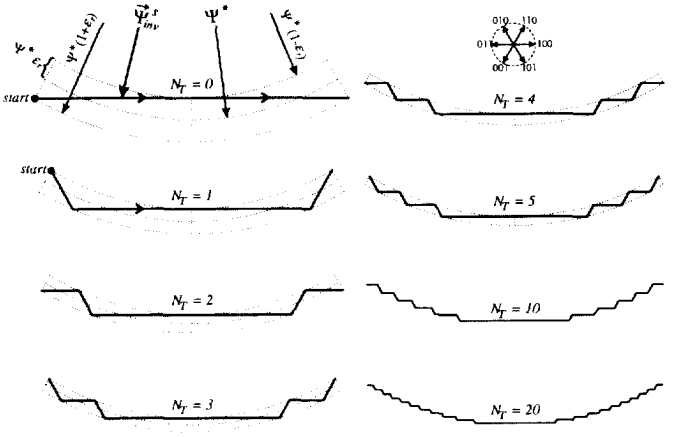

Fig. 6. 60° orbit segments of $\vec{\Psi}^s_{inv}$ with minimal radial error ε_r for $N_T \in [0,1,2,3,4,5,10,20]$, see table 1.

N_T	ε_r [%]	$T_{\min}$ [μs]	f_{sw} [Hz]
0	7.180	1253.32	>50
1	4.107	342.52	>150
2	2.889	212.63	>250
3	2.231	154.27	>350
4	1.818	120.96	>450
5	1.534	99.41	>550
8	1.048	64.64	>850
10	.863	52.35	>1050
100	.097	5.35	>10050

Table 1. Criteria to choose ε_r for U_{dc}=650 [V], U_{grid}=380 [V], f_{grid}=50 [Hz] and $\Psi^*_{inv} = \Psi_{grid}$.

executed (-60°). These two rules, keep $\vec{\Psi}^s_{inv}$ between the two tolerance circles as long as u_{dc} is sufficiently high.

The smallest possible flux increment according to (1) is $\Delta\Psi = \sqrt{\frac{2}{3}}\, U_{dc}\, T_{sw}$. Because in practise we are dealing with significant voltage ripple on u_{dc}, its highest value should be considered. The smallest allowable value of ε_r is limited by $\Delta\Psi$ and the amplitude Ψ^*_{inv}. A smaller ε_r will primarily reduce the reactive power ripple, and also increase the average switching frequency f_{sw}.

A. Flux angle control

Flux orbits as depicted in fig.6 can progress with the highest possible speed: $\frac{d\Psi}{dt} = \sqrt{\frac{2}{3}}\, U_{dc}$ when active vectors are alternated, or the flux speed can become zero when either the zero vectors 000 or 111 are chosen (see fig.1c). It is obvious that as soon as the actual flux $\vec{\Psi}^f_{inv}$ has advanced $\vec{\Psi}^{f*}_{inv}$ by a predefined amount, the best option is to stop the flux in order to minimize its deviation from the reference. For a zero vector there are two choices. Here we always take the closest one, involving only one inverter leg to switch. Once a zero vector is executed, the advancement of $\vec{\Psi}^s_{inv}$ will diminish and become negative after some time. Once $\vec{\Psi}^f_{inv}$ is behind by the same amount ε_t, the zero vector is ended, and the previous active vector is reactivated. In this way the angular error is bounded according to (21) in a very robust way.

Smooth acceleration / deceleration properties and insensitivity to u_{dc} variations result. All non-modelled effects such as turn-on and turn-off delays of the semiconductor switches are taken into account, because $\vec{\Psi}^s_{inv}$ is calculated from the actual measured inverter output voltages. It goes without saying that the duration of a zero vector should be at least T_{sw}. The tangential distance travelled by the reference during this time amounts to $\Delta\Psi^f_{inv\,b}$:

$$\Delta\Psi^f_{inv\,b} \approx \left[\sqrt{\frac{2}{3}}U_{dc} - \omega_{grid}\,\vec{\Psi}^*_{inv}(1-\varepsilon_r)\right] T_{sw} \quad (22)$$

$$\varepsilon_t \approx \frac{1}{2\vec{\Psi}^*_{inv}}\Delta\Psi^f_{inv\,b} \quad (23)$$

The four switching rules in the synchronous frame, attached to the reference flux vector, conclude to:

boundary	condition
right:	$\|\vec{\Psi}_{inv}\| \geq \Psi^*_{inv}\cdot(1+\varepsilon_r)$
left:	$\|\vec{\Psi}_{inv}\| \leq \Psi^*_{inv}\cdot(1-\varepsilon_r)$
upper:	$\Psi^f_{inv\,b} \geq \Psi^*_{inv}\cdot\varepsilon_t$
lower:	$\Psi^f_{inv\,b} \leq -\Psi^*_{inv}\cdot\varepsilon_t$

boundary	present $\vec{u}^s_{inv}$	next $\vec{u}^s_{inv}$
right:	$\vec{u}^s_{inv}$	$A_{rot}(60°)\cdot\vec{u}^s_{inv}$
left:	$\vec{u}^s_{inv}$	$A_{rot}(-60°)\cdot\vec{u}^s_{inv}$
upper:	$\vec{u}^s_{inv}$	$\vec{0}$
lower:	$\vec{0}$	$\vec{u}^s_{inv}$(before zero vect.)

Table 2. Switching rules for a rectangular fish.

B. Steady state full load performance

To proof the feasibility of the supposed control method, a comparison is made with the results from [1]. Simulations for a hard-switching 30 [kW] invertor connected to the 380 [V], 50 [Hz] grid with inductors L=2.9 [mH](0.19 p.u.) and parasitic resistance R=96 [mΩ](0.02 p.u.) and capacitor C_{dc}=2 [mF](3 p.u.) are made. In [1], LCL line filters were applied, with L =0.2p.u., C=6p.u. and f_{sw}=1.95 [kHz] (space vector modulation). It is shown that an equal or lower harmonic distortion as in [1] can be achieved at a similar (even lower) switching frequency, even though we do not use LCL filters.

During steady-state the switching rules from the table and T_{sw} =65[μs] (N_T=7) yield the phase-currents in fig.7a. Note the corresponding converter output voltages that show long durations of non-switching causing an high amount of 3rd harmonic (52%), clearly visible in the voltage spectrum in fig.8a.

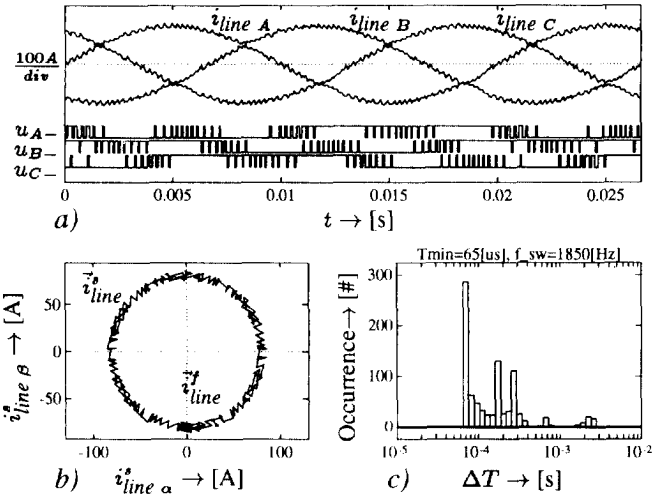

Fig. 7. Simulation: a) Full load performance of controlled rectifier (100 [A/div]). b) Current space vector and current fish $\vec{i}^{f}_{line}$. c) Switching time distribution (4 periods): minimum ΔT =65[μs].

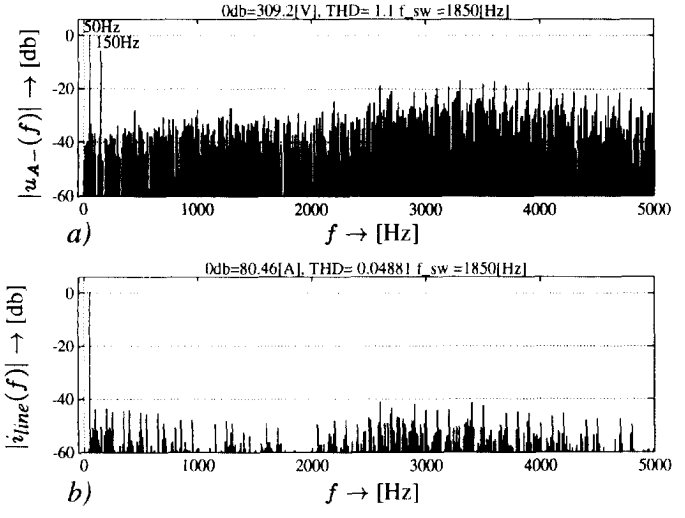

Fig. 8. Frequency spectra of converter output voltage and line-current.

The quality of the switching strategy is evident from the high occurrence of near allowable pulse widths in fig.7c and the evenly distributed current spectrum, without the abundant zero-sequence components present in u_{A-}.

C. Dynamic performance

The dynamic increase of I^* is limited by the available voltage to increase or decrease I_{line} by controlling $\vec{\Psi}^{s*}_{inv}$ to get further behind or to pass $\vec{\Psi}^{s}_{grid}$.

For $U_{dc} \approx$ 650 [V], the maximum positive $\frac{d}{dt}I_{line} \approx$ 130 [A/ms] while the negative $-\frac{d}{dt}I_{line} \approx$ 30 [A/ms]. Fig.9 clearly shows the distinct slopes of I^* due to this.

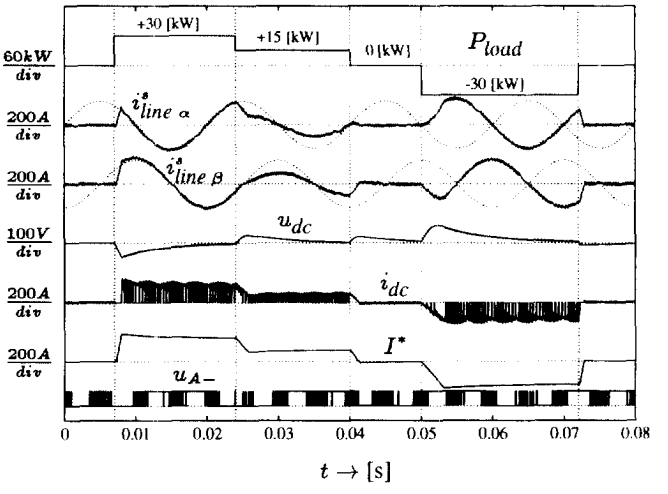

Fig. 9. Simulated transient responses of 30 [kW] PWM rectifier, while Volt-second controlled, $I^*_{react} = 0$.

The DC-link voltage gets a 30 [V] overshoot up to 680 [V] just after t = 0.05 [s], which corresponds to soving (15) for Δu_{dc}.

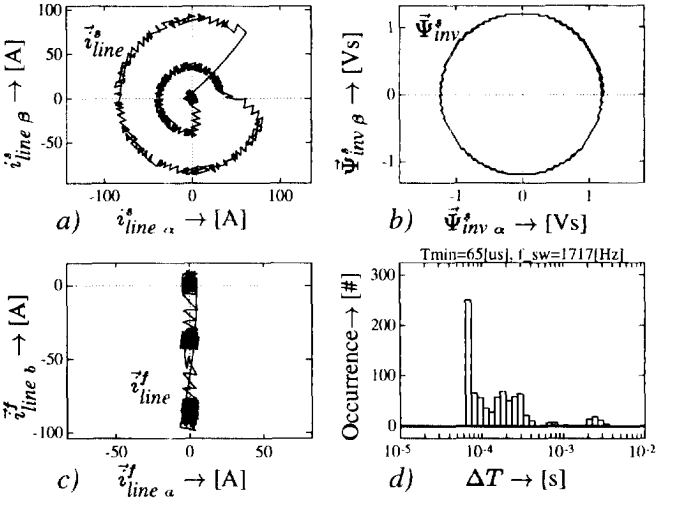

Fig. 10. First 0.05 [s] of fig.9: a) Current space vector during transients. b) Converter flux space vector c) Current fish. d) Switching times distribution for whole of fig.9.

V. Experimental results

As a test bed for a back to back 30 [kVA] a 1 [kVA] inverter was used to verify the DSP control algorithms. The small inverter is fed by a 3ϕ transformer with $U_{grid} = 143$ [V]. The link voltage is controlled to $U_{dc} = 300$ [V]. The filter component values are: C_{dc} =3 [mF], L =30 [mH], R =1.5 [Ω]. A TMSC30 DSP based digital system was used for implementing the algorithms, the required processing speed being easy to manage within a control period of 50 [μs].

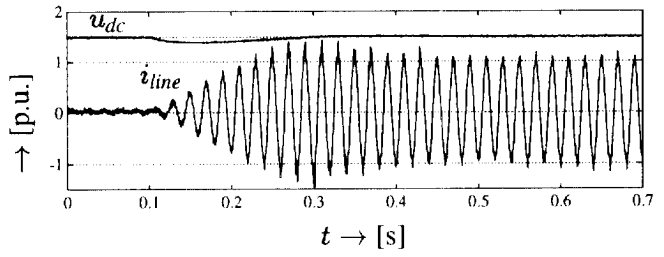

Fig. 11. Measured data: link voltage u_{dc} and line current after 100% load step.

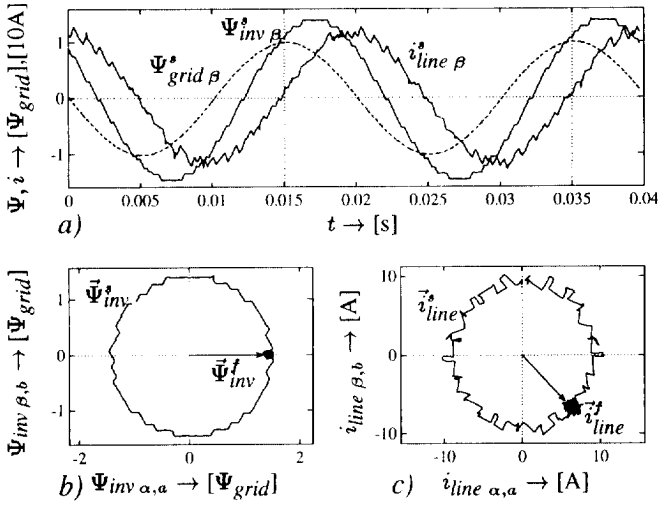

Fig. 12. Measured data: steady-state full load.

The successful operation of the flux/current controller that incorporates the techniques discussed here is shown in figs.11,12 and 13. Fig.11 concerns transient waveforms due to a load step of 100%. This measurement was made with the load power as a disturbance, i_{load} was not measured! The current response exhibits an overshoot characteristic of a PI output voltage regulator. Fig.13 shows the measured frequency spectrum of the line current in the case of fig.12. As expected, the Fish method produces a

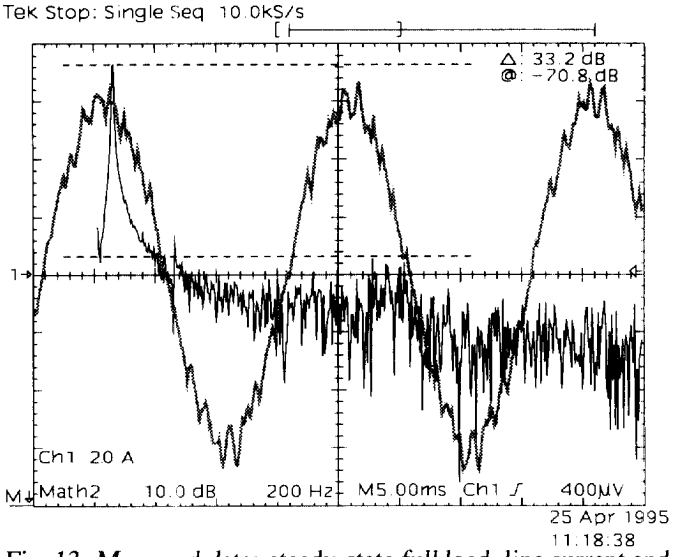

Fig. 13. Measured data: steady-state full load, line current and spectrum.

evenly spread harmonic content over a broad frequency range.

VI. Conclusions

Controlling a PWM rectifier with unity powerfactor is comparable to field oriented control of a synchronous machine with know rotor flux and infinite inertia.

Measuring line current is not required when L and R values are known. Grid-, inverter- and link voltages need to be measured to control $\vec{i}^s_{line}$ properly.

Note the extreme high content of 3rd harmonic in u_{A-}. The "smallest fish optimal switching strategy" produces a current-spectrum without the typical carrier and side-band frequencies.

References

[1] J. Ollila, "A PWM-rectifier without current measurement", EPE-journal Vol.4-no 2, June 1994.

[2] Holtz, Joachim, "Pulsewidth Modulation - A Survey", Proceedings PESC, Toledo 1992, pp 11-18.

[3] Veltman, A., P.P.J. van den Bosch, R.J.A. Gorter, "On-line Optimal Switching Patterns for 2-level and 3-level Inverters using the Fish Method", Proceedings PESC'93, Seattle 1993, pp 1063–1069.

[4] Veltman, A., P.P.J. van den Bosch, "The fish method: An analytical tool for optimizing converter-machine performance", Proceedings Power Conversion Conference, Yokohama 1993, pp. 575–580.

[5] Veltman, André, "The Fish Method, interaction between AC-Machines and Switching Power Converters", PhD. thesis, Delft University of Technology, 1994.